Spectrochimica Acta Part A: Molecular and Biomolecular Spectroscopy 303 (2023) 123239

Contents lists available at ScienceDirect

Spectrochimica Acta Part A:
Molecular and Biomolecular Spectroscopy

journal homepage: www.journals.elsevier.com/spectrochimica-acta-part-a-molecular-and-biomolecular-spectroscopy

Temperature-dependent Raman spectra and thermal expansion of MgP_2O_6

Weihong Xue [a], Bo Dai [a,b], Kuan Zhai [a,b], Haipeng Song [c], Wen Wen [d], Shuangmeng Zhai [a,*]

[a] Key Laboratory of High-temperature and High-pressure Study of the Earth's Interior, Institute of Geochemistry, Chinese Academy of Sciences, Guiyang 550081, China
[b] University of Chinese Academy of Sciences, Beijing 100049, China
[c] State Key Laboratory of Geological Processes and Mineral Resources, China University of Geosciences, Wuhan 430074, China
[d] Shanghai Synchrotron Radiation Facility, Shanghai Advanced Research Institute, Chinese Academy of Sciences, Shanghai 201210, China

HIGHLIGHTS

- Raman spectra and X-ray diffraction patterns of MgP_2O_6 were collected up to 1073 K.
- No temperature-induced phase transition occurs for MgP_2O_6.
- The effect of temperature on the Raman active vibrations of MgP_2O_6 was analyzed.
- The thermal expansion coefficients and isobaric mode Grüneisen parameters of MgP_2O_6 were determined.

GRAPHICAL ABSTRACT

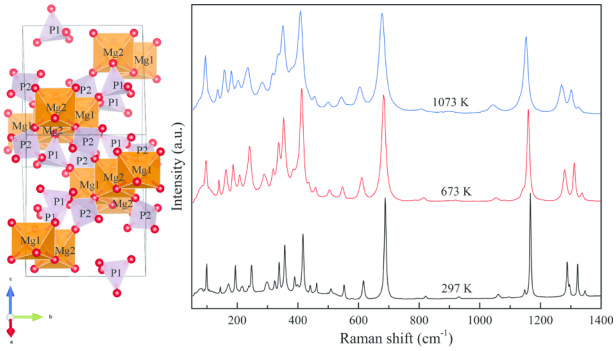

ARTICLE INFO

Keywords:
MgP_2O_6
Raman spectra
Thermal expansion
High temperature

ABSTRACT

The Raman spectra and thermal expansion of MgP_2O_6 metaphosphate were investigated at various temperatures up to 1073 K at ambient pressure. No temperature-induced phase transition was observed in this study. The effect of temperature on the Raman active vibrations and unit cell parameters was determined. All the observed Raman active bands of MgP_2O_6 showed linear temperature dependences in the range of $-2.61 \times 10^{-2} \sim -0.49 \times 10^{-2}$ cm^{-1} K^{-1}. The thermal expansion coefficient of MgP_2O_6 was estimated to be 3.21(2) $\times$ 10^{-5} K^{-1}. An axial anisotropic thermal expansion exists and the *c*-axis shows the smallest thermal expansion. The isobaric mode Grüneisen parameters of MgP_2O_6 were calculated. The obtained results were compared with other compounds in the MgO-P_2O_5 system.

1. Introduction

The metaphosphates with the chemical formula of AP_2O_6 (A = divalent cation) contain a number of compounds. Due to their potential technical and material applications, such as luminescence, dielectric, biomaterial, and catalysis, metaphosphates have been intensively investigated [1–10]. Mainly there are three kinds of crystal structures for AP_2O_6 metaphosphates with different divalent cations, including monoclinic CuP_2O_6-type (space group: *C2/c*, e.g., A = Mg, Cu, Ni, Co, Fe, Mn) and CaP_2O_6-type (space group: $P2_1/c$, e.g., A = Ca, Sr, Ba, Pb), and

* Corresponding author.
E-mail address: zhaishuangmeng@mail.gyig.ac.cn (S. Zhai).

https://doi.org/10.1016/j.saa.2023.123239
Received 2 July 2023; Received in revised form 28 July 2023; Accepted 4 August 2023
Available online 6 August 2023

orthorhombic CdP_2O_6-type (space group: *Pbca*, e.g., A = Cd, Hg) [11]. Additionally, a high- temperature form of CdP_2O_6 also belongs to the orthorhombic structure (space group: $P2_12_12_1$) [11].

Magnesium metaphosphate, MgP_2O_6, is one of the four compounds in MgO-P_2O_5 binary system [12–13]. The crystal structure of monoclinic MgP_2O_6 was determined in previous studies [14–15], as shown in Fig. 1. In MgP_2O_6 two kinds of Mg with six-fold coordination exist and slightly disordered MgO_6 octahedra in the interlayer space share edges, and two kinds of P with four-fold coordination form corner-sharing PO_4 tetrahedra, which are linked together in a ring to form $P_4O_{12}^{4-}$ anions by P-O-P bridges [15]. The three-dimensional framework of MgP_2O_6 is constructed by $P_4O_{12}^{4-}$ anionic groups connected via MgO_6 octahedra.

In previous studies [2,16–21], the melting points of MgP_2O_6 were reported around 1438 K by differential thermal analysis and quenching experiments, and no temperature-induced phase transition was observed. However, there is little information about the vibrational and thermal expansion properties of MgP_2O_6 at various temperatures.

In MgO-P_2O_5 binary system, there are four compounds including $Mg_3(PO_4)_2$, $Mg_2P_2O_7$, MgP_2O_6 and MgP_4O_{11} [12–13]. In our previous studies, the thermal expansions and temperature-dependent Raman spectra of $Mg_3(PO_4)_2$ and $Mg_2P_2O_7$ have been investigated [22–23]. In this study, by using Raman spectroscopic and in-situ X-ray diffraction (XRD) measurements, the Raman spectra and thermal expansion of MgP_2O_6 were investigated up to 1073 K at ambient pressure. The effects of temperature on Raman active modes and the lattice parameters of MgP_2O_6 were quantitatively analyzed. Additionally, the thermal behavior of MgP_2O_6 was compared with other compounds in the MgO-P_2O_5 system.

2. Experimental

A pure MgP_2O_6 sample was synthesized by a conventional solid-state chemical reaction at 1273 K for 72 h using proportional high pure MgO and $NH_4H_2PO_4$ reagents (99.99% in mass fraction) purchased from Shanghai Aladdin Biochemical Technology Co., Ltd, China. The synthetic MgP_2O_6 was characterized by powder X-ray diffraction and confirmed as a single phase.

Raman spectra of MgP_2O_6 at temperatures up to 1073 K and ambient pressure were collected by a Horiba LabRam HR Evolution Raman spectrometer equipped with an 1800 gr/mm grating. The procedure was same as our previous studies [22–24]. A pulsed YAG: Nd^{3+} laser beam with 532-nm wavelength and 100-mW power was adopted as an excitation source. Through a 100× objective lens, the spot of Raman scattering light on the sample surface was about 1 μm^2. A thin small piece of MgP_2O_6 was put on a sapphire window which was placed into an alumina chamber in a Linkam TS 1500 high temperature stage for heating. An S-type thermocouple was used to measure the temperatures which were completely automatically and programmatically controlled to change and maintain any desired temperature. For thermal equilibrium in measurements, each Raman spectrum was recorded after keeping at the desired temperature for at least 5 min. The Raman shift was calibrated by plasma and neon emission lines with an accuracy of ± 1 cm^{-1}. The accumulation time for each spectrum was 30 s, and the obtained spectrum was the average of three measurements. The Raman spectra were analyzed using the PeakFit program (SPSS Inc., Chicago) to obtain a reasonable approximation.

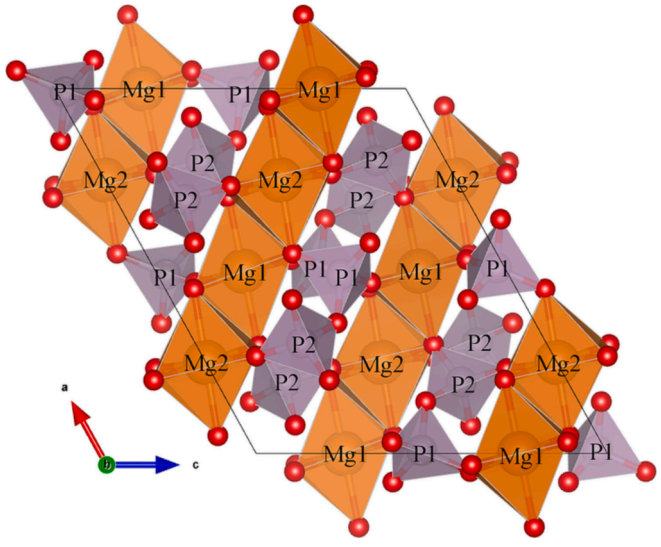

Fig. 1. The crystal structure of MgP_2O_6. The red balls represent oxygen. (For interpretation of the references to colour in this figure legend, the reader is referred to the web version of this article.)

High-temperature in-situ powder X-ray diffraction experiments were carried out from room temperature to 1073 K at the BL14B1 beam line of Shanghai Synchrotron Radiation Facility (SSRF) [25]. The method was same as our previous studies [22–23]. The synthetic MgP_2O_6 powder was loaded into a fused quartz capillary (inner diameter of 0.5-mm) which was centered at a custom-made furnace for heating and the temperature was measured by a K-type thermocouple. The wavelength of the X-ray beam (beam size = 180 × 200 μm^2) with an energy of 18 keV was calibrated by the LaB_6 standard from NIST (660b). In-situ XRD patterns were collected using a Mythen 1 K linear detector in Debye-Sherrer mode [26]. For thermal equilibration, each temperature was kept for about 5 min before measuring. The lattice parameters of MgP_2O_6 at different temperatures were obtained by using the full profile-fitting technique in EXPGUI/GSAS [27–28].

3. Results and discussion

As mentioned above, the crystal structure of monoclinic MgP_2O_6 is in the space group of *C2/c* with $Z = 4$. According to the factor group analysis [29], the Raman active modes of MgP_2O_6 are as following:

$\Gamma = 25A_g + 26B_g$.

Therefore, totally 51 Raman active modes MgP_2O_6 are predicted. However, due of the overlapping and/or low intensity of some Raman active modes, the number of observed Raman peaks is less than the expected.

As shown in Fig. 2, 29 bands can be distinguished in the Raman spectrum collected at ambient conditions, which is consistent with the previous study [30]. According to previous studies [10,30], the Raman active modes can be ascribed to the vibrations of the $P_4O_{12}^{4-}$ anionic groups involving P-O-P and = PO_2. As listed in Table 1, the observed Raman vibrations of MgP_2O_6 were assigned based on previous reports [10,30]. It is noted that the vibrations of MgP_2O_6 are more complicated than those of $Mg_2P_2O_7$ involving $P_2O_7^{4-}$ anions and $Mg_3(PO_4)_2$ involving PO_4^{3-} anions. It is known that the crystal structure is an important factor for the observed Raman bands of a material, even if the involving elements are the same but in different arrangement. The compounds in MgO-P_2O_5 system contain basic Mg-O polyhedra and PO_4 tetrahedra with different arrangements. MgP_2O_6 is monoclinic with space group of *C2/c* where corner-sharing PO_4 tetrahedra form $P_4O_{12}^{4-}$ anions by P-O-P bridges and connect via MgO_6 octahedra [15]. α- and β-$Mg_2P_2O_7$ are monoclinic with different space groups of $P2_1/c$ and *C2/m* [31–32]. In α-$Mg_2P_2O_7$ the $[P_2O_7]^{4-}$ groups lie between edge-sharing MgO_5 and MgO_6 polyhedral sheets parallel to the *ab* plane [31]. In β-$Mg_2P_2O_7$ the $[P_2O_7]^{4-}$ groups linearly lie between the MgO_6 octahedral sheets [32]. There is a difference for the $[P_2O_7]^{4-}$ anion in α- and β-$Mg_2P_2O_7$ since the P-O-P bond angle is 144° in α-$Mg_2P_2O_7$ [31] but 180° in β-$Mg_2P_2O_7$ [32]. $Mg_3(PO_4)_2$-I and $Mg_3(PO_4)_2$-II are monoclinic with space group of $P2_1/n$, where PO_4^{3-} anions in $Mg_3(PO_4)_2$-I are linked by an identical layer consisting MgO_5 polyhedra and MgO_6 polyhedra, while PO_4^{3-} anions in $Mg_3(PO_4)_2$-II are linked by two inequivalent layers consisting two consistent MgO_6 polyhedra and stacking along the *b*-axis [33–34].

Table 1
Constants determined in $\nu_i = \nu_0 + b_i T$ of MgP_2O_6 at ambient pressure.

No.	ν_{i0}	$-b_i \times 10^2$	R^2	γ_{iP}	$b_i/\nu_{i0} \times 10^5$	ν_{297}	Assignment
1	1355.3(3)	2.61(4)	0.995	0.60	-1.93	1347.0(1)	$\nu_{as}(PO_2)$
2	1330.7(1)	2.70(2)	0.999	0.63	-2.03	1322.6(1)	
3	1302.3(3)	2.10(9)	0.988	0.50	-1.61	1296.2(1)	
4	1294.8(3)	2.16(5)	0.992	0.52	-1.67	1288.1(1)	
5	1172.9(2)	1.82(3)	0.994	0.48	-1.55	1166.9(1)	$\nu_s(PO_2)$
6	1153.0(1)	1.66(2)	0.997	0.45	-1.44	1147.9(1)	
7	1067.8(5)	2.08(7)	0.980	0.61	-1.95	1060.9(2)	$\nu_{as}(POP)$
8	938.7(8)	2.51(13)	0.969	0.83	-2.67	930.6(3)	
9	825.8(2)	1.54(3)	0.994	0.58	-1.86	821.2(2)	$\nu_s(POP)$
10	692.3(2)	1.36(2)	0.996	0.61	-1.96	687.9(1)	
11	620.9(2)	1.54(2)	0.997	0.77	-2.48	616.2(1)	PO_2 bend POP bend
12	555.7(1)	1.16(2)	0.995	0.65	-2.09	552.2(1)	
13	512.6(2)	1.17(2)	0.993	0.71	-2.28	509.2(4)	
14	463.4(1)	0.75(2)	0.989	0.50	-1.62	461.5(2)	
15	443.0(2)	0.93(4)	0.977	0.65	-2.10	440.6(2)	
16	419.4(1)	0.95(2)	0.994	0.71	-2.27	416.7(1)	
17	400.9(7)	0.49(8)	0.863	0.38	-1.22	399.8(5)	
18	392.2(3)	1.12(8)	0.928	0.89	-2.86	389.2(2)	
19	359.1(1)	0.78(1)	0.997	0.68	-2.17	356.8(1)	
20	339.8(1)	0.57(3)	0.960	0.52	-1.68	338.0(1)	
21	325.8(2)	0.96(2)	0.989	0.92	-2.95	323.5(2)	
22	303.7(2)	2.01(2)	0.998	2.06	-6.62	298.2(3)	
23	251.1(1)	1.43(2)	0.997	1.77	-5.69	247.1(1)	
24	241.9(3)	1.64(6)	0.981	2.11	-6.78	237.2(5)	
25	219.4(3)	1.57(3)	0.993	2.23	-7.16	215.9(3)	
26	198.6(1)	1.69(1)	0.999	2.65	-8.51	193.7(1)	
27	173.5(3)	1.48(3)	0.994	2.66	-8.53	170.8(3)	
28	147.3(1)	1.09(2)	0.997	2.31	-7.40	144.0(2)	
29	100.5(1)	0.55(1)	0.996	1.70	-5.47	99.1(1)	

ν_{i0} and ν_{297} is in cm^{-1}, T in K, the constants b_i and b_i/ν_{i0} have the corresponding units. R^2 is the correlation coefficient.

ν_{i0} and ν_{297} is in cm^{-1}, T in K, the constants b_i and b_i/ν_{i0} have the corresponding units. R^2 is the correlation coefficient.

$Mg_3(PO_4)_2$-III is triclinic with space group of *P-1* consisting of four inequivalent PO_4^{3-} anions linked by sharing corners and edges to distorted MgO_4, MgO_5 and MgO_6 polyhedra [35].

3.1. Temperature-dependent Raman spectra of MgP_2O_6

The Raman spectra of MgP_2O_6 at various temperatures were shown in Fig. 2. Most Raman peaks can be distinguished even at high temperatures. It is clear that the Raman active vibrations shift to lower frequency regions during heating. It is logical since the bond length becomes larger with heating, indicating weaker bond, i.e., small force constant, and consequent lower vibrational frequency according to Hooke's law. No new Raman peak appears during heating to 1073 K though one or two peaks become undistinguished at high temperatures due to the overlapping or low intensity, indicating no phase transition. As mentioned above, the melting temperature is about 1438 K, which is higher than 1073 K. Therefore, no melting behavior can be observed in this study.

The variations of Raman shift of vibrations at different temperatures for MgP_2O_6 were plotted in Fig. 3. The constants derived by linear regressions were listed in Table 1. The temperature coefficients (b_i) of vibrations in MgP_2O_6 are negative and vary from -2.66 to -0.38×10^{-2} cm^{-1} K^{-1}. Generally, the stretching vibrations of MgP_2O_6 (including $\nu_{as}(PO_2)$, $\nu_s(PO_2)$, $\nu_{as}(POP)$ and $\nu_s(POP)$) show larger absolute

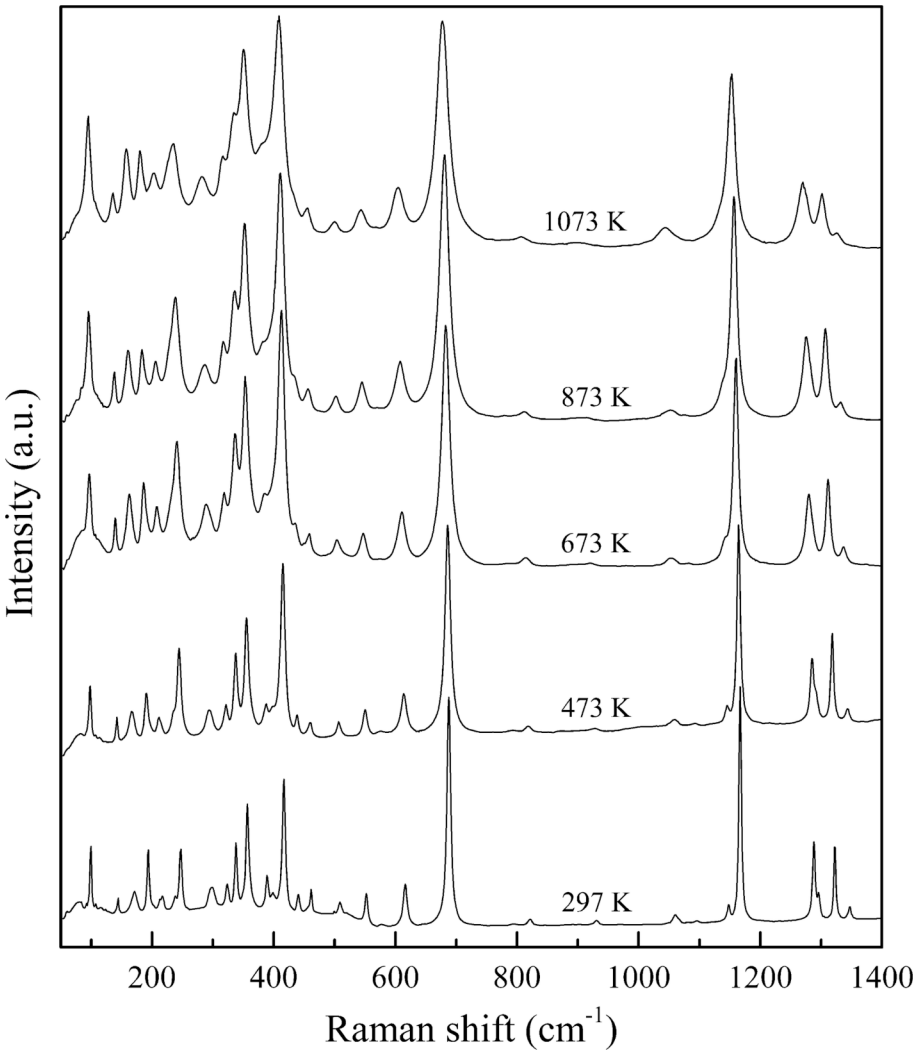

Fig. 2. Typical Raman spectra of MgP_2O_6 up to 1073 K at ambient pressure.

temperature-dependence, whereas the PO_2 and P-O-P bending modes show smaller absolute temperature-dependence. On the other hand, as described in a previous study of Mishra et al. [36], a reduced slope ($1/\omega_i\ \partial\omega_i/\partial T$, as b_i/ν_{i0} in Table 1) representing the normalized value of the temperature dependence of mode frequencies can be used to decide the sensitivity of Raman modes with temperature. As listed in Table 1, the calculated reduced slopes are negative and in the range of $-1.22 \sim -8.53 \times 10^{-5}$ K^{-1}. The PO_2 and POP bending modes show larger reduced slopes, especially the modes less than 300 cm^{-1}, than those of stretching vibrations. It means that these bending modes are sensitive to temperature.

3.2. Thermal expansion of MgP_2O_6

Fig. 4 shows the typical XRD patterns of MgP_2O_6 from room temperature to 1073 K. With heating, the XRD peaks shift to low 2θ region. It is reasonable since the *d*-spacing expands during heating, resulting in decreasing θ according to Bragg's law. Similar to the high-temperature Raman spectroscopic study, there is no new appearing X-ray diffraction peak during heating to 1073 K, implying no phase change. As examples, the refinements of XRD patterns collected at room temperature, 673 K and 1073 K are illustrated in Fig. 5. And the obtained lattice parameters of MgP_2O_6 at various temperatures are listed in Table 2. The variations of the unit-cell parameters (*a, b, c, V*) for MgP_2O_6 are plotted in Fig. 6.

The thermal expansion coefficient $\alpha_v = 1/V\ (\partial V/\partial T)$, was defined to express the fluctuation of lattice parameters as a function of temperature. If the thermal expansion coefficient α_v does not change with temperature, integration gives the following expression [37]:

$$\ln(V/V_0) = \alpha_v(T - T_0)$$

In the same way, the axial thermal expansion coefficients along the *a*-, *b*- and *c*-axis can be obtained by the following expressions:

$$\ln(a/a_0) = \alpha_a(T - T_0)$$

$$\ln(b/b_0) = \alpha_b(T - T_0)$$

$$\ln(c/c_0) = \alpha_c(T - T_0).$$

Using the lattice parameters listed in Table 2 and the above expressions, the thermal expansion coefficients of MgP_2O_6 are calculated as $3.21(2) \times 10^{-5}$ K^{-1}, $1.47(2) \times 10^{-5}$ K^{-1}, $1.25(5) \times 10^{-5}$ K^{-1} and $0.39(3) \times 10^{-5}$ K^{-1} for *V*, *a*-, *b*- and *c*-axis, respectively, as listed in Table 3. Obviously, axial thermal expansion anisotropy exists in MgP_2O_6 since the *a*- and *b*-axis show larger thermal expansion coefficients than that of the *c*-axis. It is reasonable since the atomic arrangements along the *a*- and *b*-axis are looser than those along the *c*-axis.

Table 3 also shows the thermal expansion coefficients of other compounds in the $MgO\text{-}P_2O_5$ system. Due to different structures and atomic arrangements, these compounds show different bulk and axial

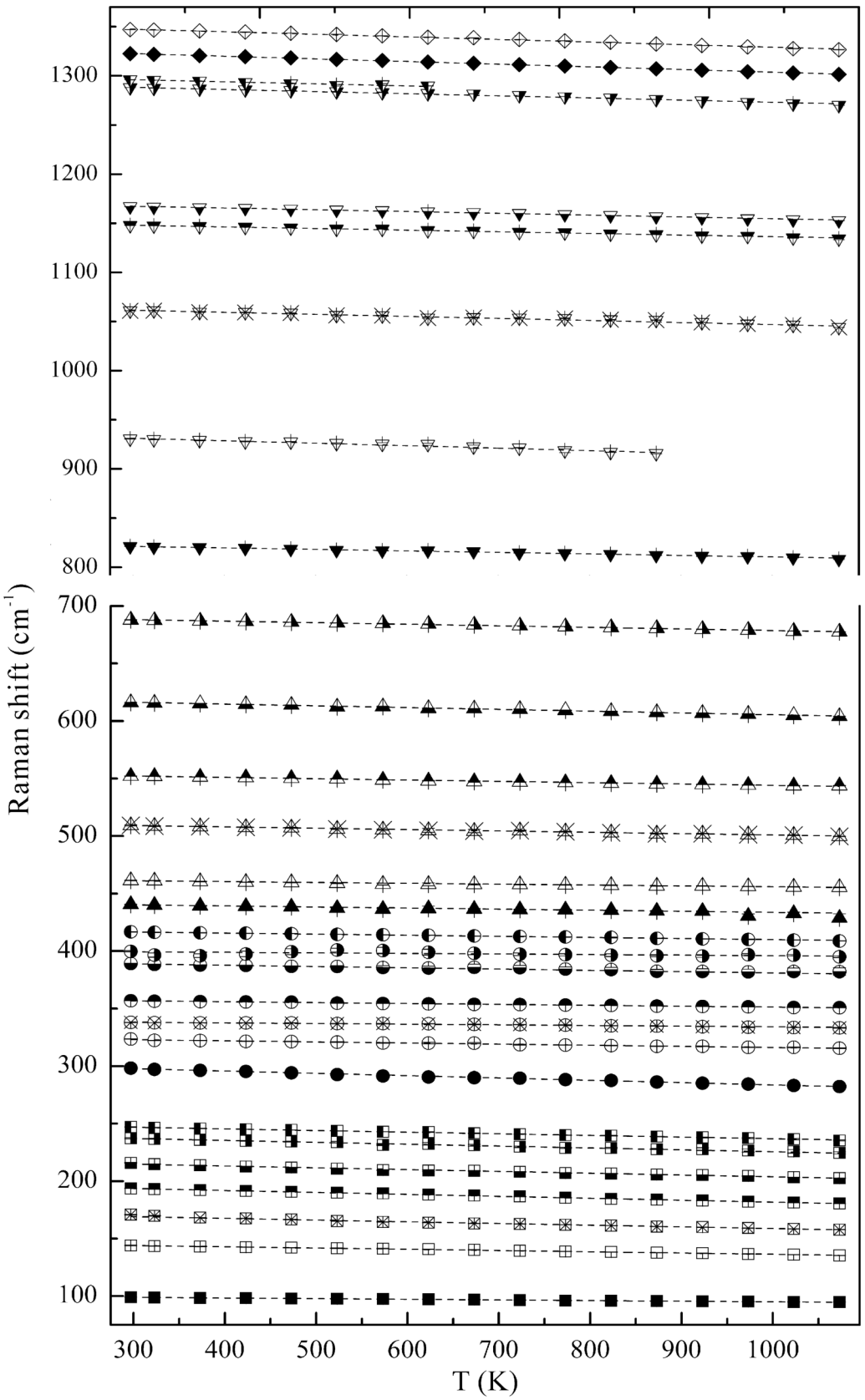

Fig. 3. Temperature dependence of the Raman active vibrations for MgP_2O_6 at ambient pressure.

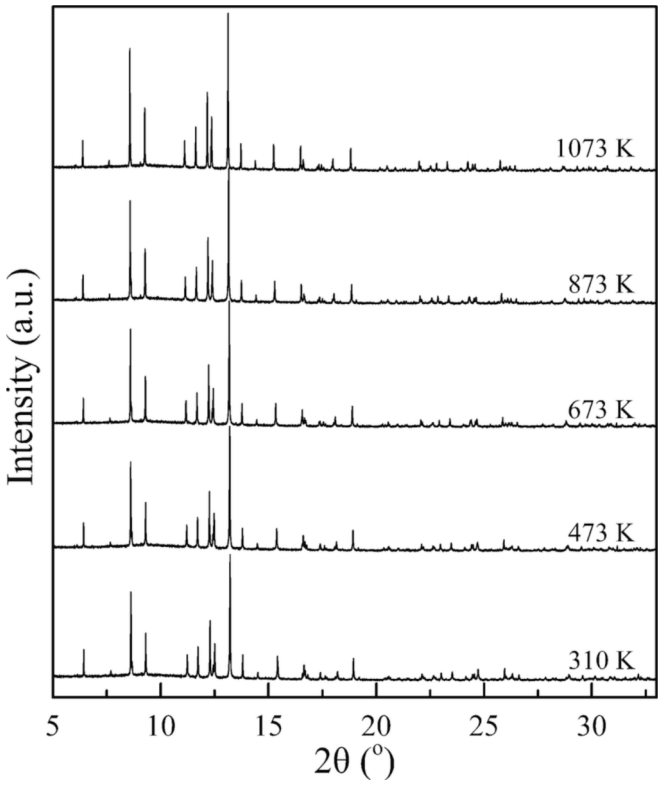

Fig. 4. Typical XRD patterns of MgP_2O_6 up to 1073 K at ambient pressure.

thermal expansion behaviors. MgP_2O_6 contains $P_4O_{12}^{4-}$ anionic groups and MgO_6 octahedra, β-$Mg_2P_2O_7$ includes $P_2O_7^{4-}$ anionic groups and MgO_6 octahedra, and $Mg_3(PO_4)_2$ polymorphs involve PO_4^{3-} anionic groups and different Mg-O polyhedra.

3.3. Isobaric mode Grüneisen parameters

Based on the temperature-dependent Raman spectra and thermal expansion coefficient, the isobaric mode Grüneisen parameters (γ_{iP}) of MgP_2O_6 can be calculated by using the following formula [38–39]:

$$\gamma_{iP} = -\frac{1}{\alpha}\left(\frac{\partial \ln \nu_i}{\partial T}\right)_P$$

where α is the volume thermal expansion coefficient, as 3.21(2) × 10^{-5} K^{-1} obtained in this study.

The calculated values of γ_{iP} for different $P_4O_{12}^{4-}$ vibrational modes of MgP_2O_6 are also listed in Table 1, which are in the range of 0.38–2.66, and the averaged isobaric mode Grüneisen parameter is 1.06. It is noted that the mode Grüneisen parameter for the low frequency modes (100–300 cm^{-1}) are with high values, as listed in Table 1. Indeed, $\gamma_{iP} = -b_i/\nu_{i0}/\alpha_v$.. Therefore, the larger reduced slopes of the low frequency modes (100–300 cm^{-1}) result in higher mode Grüneisen parameters, which also mean that these modes are sensitive to temperature. In our previous study [23], the γ_{iP} for $P_2O_7^{4-}$ vibrational modes of β-$Mg_2P_2O_7$ are in the range of 0.27–1.86 with an average of 0.77. The γ_{iP} for PO_4^{3-} vibrational modes of $Mg_3(PO_4)_2$ polymorphs (I, II, III) are 0.35–0.84, 0.31–0.57, and 0.07–1.33 with averages of 0.54, 0.40, and 0.51, respectively [22]. The discrepancy might be contributed to the structural evolution of the PO_4 tetrahedra during heating in different anionic groups, i.e., $P_4O_{12}^{4-}$, $P_2O_7^{4-}$ and PO_4^{3-}, which is also related to the crystal structure (arrangement of atoms) and thermal expansion.

4. Conclusions

In this study, the Raman spectra and X-ray diffraction patterns of

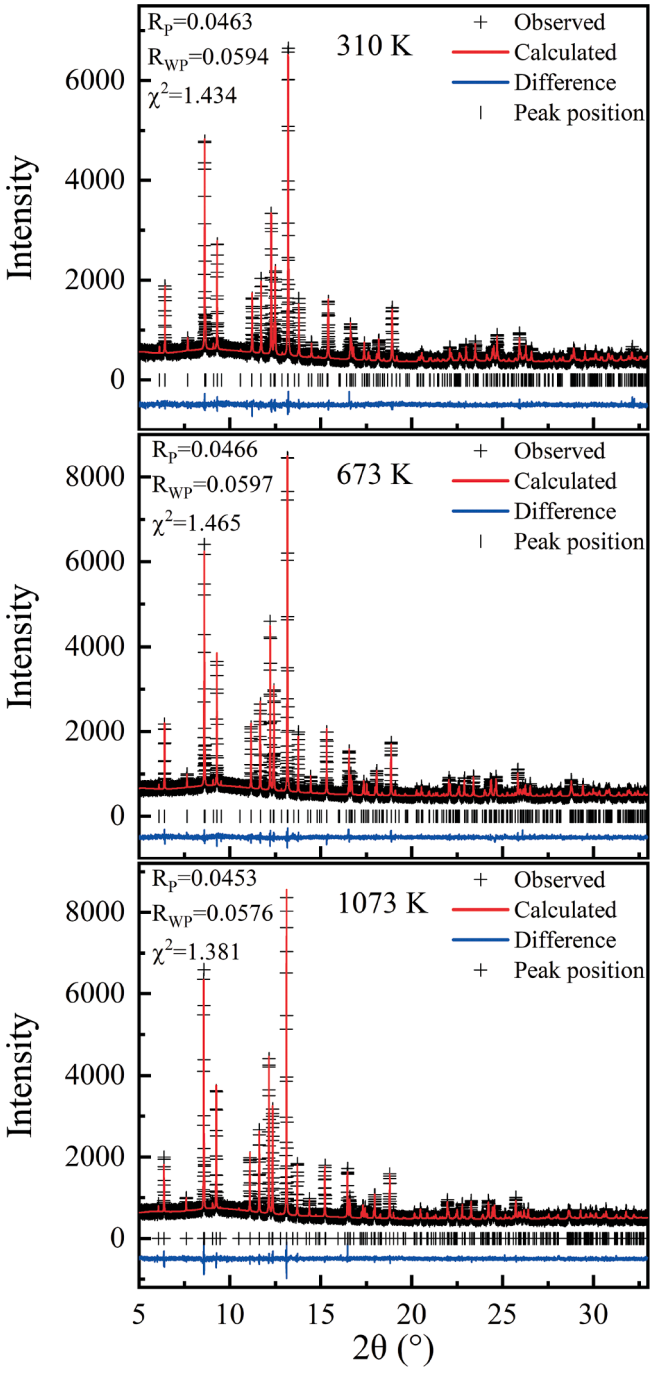

Fig. 5. Refined X-ray diffraction patterns of MgP_2O_6 collected at room temperature, 673 K and 1073 K. Black crosses represent the observed XRD pattern, red line, bottom blue curve and red bars are the calculated XRD pattern, the difference and peak positions determined by Rietveld analysis. The respective Rp, Rwp and χ^2 values were also included. (For interpretation of the references to colour in this figure legend, the reader is referred to the web version of this article.)

MgP_2O_6 were measured from room temperature to 1073 K at ambient pressure. No temperature-induced phase transformation was observed. The Raman shifts of all observed vibrations for MgP_2O_6 continuously and linearly decrease with increasing temperature in the dependences of $-2.61 \times 10^{-2} \sim -0.49 \times 10^{-2}$ cm^{-1} K^{-1}. The thermal expansion coefficient of MgP_2O_6 was determined as 3.21(2) × 10^{-5} K^{-1} and an axial anisotropic thermal expansion exists since the thermal expansion coefficients for *a*-, *b*- and *c*-axis are 1.47(2) × 10^{-5} K^{-1}, 1.25(5) × 10^{-5} K^{-1}

Table 2
Lattice parameters of MgP_2O_6 at various temperatures and ambient pressure.

T (K)	a (Å)	b (Å)	c (Å)	β (°)	V (Å^3)
310	11.7324(2)	8.2628(2)	9.9251(2)	118.905(1)	842.3(5)
373	11.7446(2)	8.2697(2)	9.9252(2)	118.905(1)	843.9(1)
473	11.7620(1)	8.2796(1)	9.9269(1)	118.898(1)	846.4(1)
573	11.7806(1)	8.2902(1)	9.9315(1)	118.889(1)	849.2(1)
673	11.7985(1)	8.3011(1)	9.9350(1)	118.880(1)	852.0(1)
773	11.8160(1)	8.3121(1)	9.9422(1)	118.866(1)	855.1(1)
873	11.8271(2)	8.3213(1)	9.9449(1)	118.844(1)	857.3(1)
973	11.8456(1)	8.3310(1)	9.9523(1)	118.834(1)	860.4(1)
1073	11.8620(1)	8.3419(1)	9.9598(1)	118.819(1)	863.5(1)

Standard deviations are in parentheses.

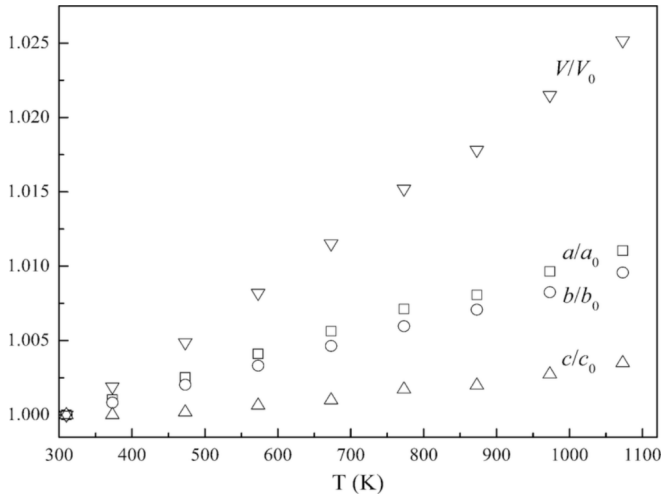

Fig. 6. Relative variations of unit-cell parameters with temperature for MgP_2O_6.

Table 3
Thermal expansion ($\times 10^{-5}$ K^{-1}) of compounds in the MgO-P_2O_5 system.

Compound	Space group	a_a	a_b	a_c	a_v	Ref.
MgP_2O_6	*C2/c*	1.47 (2)	1.25 (5)	0.39 (3)	3.21 (2)	This study
β-MgP_2O_7	*C2/m*	1.48 (7)	1.02 (1)	0.78 (3)	2.97 (8)	Xue et al. (2022)
$Mg_3(PO_4)_2$-I	*P2$_1$/n*	1.04 (1)	2.06 (3)	0.21 (3)	3.31 (4)	Hu et al. (2022)
$Mg_3(PO_4)_2$-II	*P2$_1$/n*	1.42 (1)	1.34 (1)	1.16 (1)	3.91 (4)	Hu et al. (2022)
$Mg_3(PO_4)_2$-III	*P-1*	1.09 (1)	1.57 (2)	1.21 (2)	3.25 (5)	Hu et al. (2022)

Standard deviations are in parentheses.

and 0.39(3) × 10^{-5} K^{-1}, respectively. The isobaric mode Grüneisen parameters of MgP_2O_6 were calculated in the range of 0.38–2.66 with an average of 1.06.

CRediT authorship contribution statement

Weihong Xue: Investigation, Writing – original draft. **Bo Dai:** Data curation. **Kuan Zhai:** Data curation. **Haipeng Song:** Data curation. **Wen Wen:** Methodology, Resources, Funding acquisition. **Shuangmeng Zhai:** Conceptualization, Writing – review & editing, Funding acquisition.

Declaration of Competing Interest

The authors declare that they have no known competing financial interests or personal relationships that could have appeared to influence the work reported in this paper.

Data availability

Data will be made available on request.

Acknowledgements

The authors thank Prof. Judy Kim for the editorial handling and two anonymous referees for their constructive reviews. This work was financially supported by the National Natural Science Foundation of China (Grant Nos. 42120104005 and U1932201), Chinese Academy of Sciences (Grant No. 132852KYSB20200011), Photon Science Research Center for Carbon Dioxide, and Guizhou Provincial 2021 Science and Technology Subsidies (No. GZ2021SIG). The in-situ synchrotron X-ray diffraction measurements were carried out at the BL14B1 beamline of the Shanghai Synchrotron Radiation Facility (Proposal No. 2022-SSRF-PT-500810).

References

[1] D.G. Engle, B.S. Hopkins, Studies in luminescence, J. Opt. Soc. Am. 11 (1925) 599–615.
[2] J.F. Sarver, F.A. Hummel, Phase equilibria and fluorescence in the system Zn$(PO_3)_2$-Mg$(PO_3)_2$, J. Electrochem. Soc. 106 (1959) 500–504.
[3] J.J. Brown, F.A. Hummel, Phase equilibria and manganese-activated luminescence in portions of the system Zn$(PO_3)_2$-Cd$(PO_3)_2$-Mg$(PO_3)_2$, J. Electrochem. Soc. 111 (1964) 660–665.
[4] S. Parke, R.S. Webb, Optical properties of Sn^{2+} and Sb^{3+} in calcium metaphosphate glass, J. Phys. D 4 (1971) 825–828.
[5] H.M.J.M. van Ass, J.M. Stevels, Internal friction and dielectric losses of mixed alkali alkaline-earth metaphosphate glasses, J. Non-Cryst. Solids 16 (1974) 267–280.
[6] E. Park, Y. Lee, J. Choi, S. Oh, H. Shin, K. Kim, S. Kim, Cellular biocompatibility and stimulatory effects of calcium metaphosphate on osteoblastic differentiation of human bone marrow-derived stromal cells, Biomaterials 25 (2004) 3403–3411.
[7] R. Hussin, S. Hamdan, D. Halim, M. Husin, The origin of emission in strontium magnesium pyrophosphate doped with Dy_2O_3, Mater. Chem. Phys. 121 (2010) 37–41.
[8] T. Klamrassamee, N. Laosiripojana, K. Faungnawakij, L. Moghaddam, Z. Zhang, W. O. Doherty, Co-and Ca-phosphate-based catalysts for the depolymerization of organosolv eucalyptus lignin, RSC Adv. 5 (2015) 45618–45621.
[9] R. Mahajan, R. Prakash, Effect of Eu^{3+} activator on spectral investigation of red emitting MgP_2O_6 phosphate, Optik 266 (2022), 169611.
[10] D. Wei, X. Yang, Y. Liu, H.J. Seo, Structural and optical properties of $Mg_{1-x}Mn_xP_2O_6$ (x = 0–1.0) magnesium metaphosphate, J. Am. Ceram. Soc. 106 (2023) 4246–4260.
[11] H.S. Ra, Strukturchemische Untersuchungen an AB_2O_6 Oxiden und Untersuchungen zur photokatalytischen Aktivität ausgewählter Verbindugnen dieses Typs: (A= Ba, Ca, Co, Cu, Eu, Fe, Mg, Mn, Ni, Pb, Sn, Sr, Zn; B= V, Nb, Ta), Universität des Saarlandes, 2009.
[12] G.G. Curiel, Thermodynamic Modeling of MgO-P_2O_5, MnO-P_2O_5 and CaO-MgO-P_2O_5 Systems, McGill University Libraries, 2013.
[13] G. Ding, W. Xie, I. Jung, Z. Qiao, G. Du, Z. Cao, Thermodynamic assessment of the MgO-P_2O_5 and CaO-P_2O_5 systems, Acta Phys.-Chim. Sin. 31 (2015) 1853–1863.
[14] M. Beucher, J.C. Grenier, Donnees cristallographiques sur les tetrametaphosphates du type $M^{II}_2P_4O_{12}$ (M^{II} = Ni, Mg, Zn, Cu Co, Mn), Mat. Res. Bull. 3 (1968) 643–647.
[15] A. Nord, K.B. Lindberg, The crystal structure of magnesium tetrametaphosphate, Acta Chem. Scand. A 29 (1975) 1–6.
[16] E. Thilo, I. Grunze, Zur chemie der kondensierten phosphate und arsenate. XV. Produkte und verlauf der entwässerung saurer phosphate der zweiwertigen lonen des Mg, Mn, Fe, Co, Ni, Cu, Zn, Cd und Hg, Z. Anorg. Allg. Chem. 290 (1957) 209-222.
[17] J. Berak, The system magnesium oxide—phosphorus pentoxide, Rocz. Chem. 32 (1958) 17–22.
[18] R. Andrieu, R. Diament, Etude des systems binaires metaphosphate de potassium-metaphosphate de calcium et metaphosphate de potassium- metaphosphate de magnesium, Compt. Rend. 259 (1964) 4708–4711.
[19] B. Thonnerieux, J.C. Grenier, A. Durif, C. Martin, JCPDS Card No. 22-477, CR Seances Acad. Sci., Ser. C 267 (1968) 968-970.
[20] E. Rakotomahanina-Rolaisoa, Y. Henry, A. Durif-Varambon, C. Raholison, Étude des systèmes $TlPO_3$-Co$(PO_3)_2$, $TlPO_3$-Mg$(PO_3)_2$ et $TlPO_3$-Ca$(PO_3)_2$, Bull. Soc. Fr. Mineral. Cristallogr. 93 (1970) 43–51.

[21] G. Czupińska, Phase equilibria in the system YPO_4-$Mg(PO_3)_2$, Thermochim. Acta 202 (1992) 77–80.
[22] X. Hu, K. Zhai, M. Jia, Y. Liu, X. Wu, W. Wen, W. Xue, S. Zhai, Phase transition of $Mg_3(PO_4)_2$ polymorphs at high-temperature: In-situ synchrotron X-ray diffraction and Raman spectroscopic study, Spectrochim. Acta A 269 (2022), 120762.
[23] W. Xue, K. Zhai, H. Wang, X. Wu, W. Wen, S. Zhai, Raman spectroscopic and X-ray diffraction study of α- and β-$Mg_2P_2O_7$ at various temperatures, Spectrochim. Acta A 273 (2022), 121076.
[24] S. Zhai, B. Dai, W. Xue, J.D. Rumney, H. Wang, S.R. Shieh, X. Wu, Pressure-and temperature-dependent Raman spectra of $Ca_2Fe_2O_5$ oxygen defect perovskite, Spectrochim. Acta A 279 (2022), 121436.
[25] T. Yang, W. Wen, G. Yin, X. Li, M. Gao, Y. Gu, L. Li, Y. Liu, H. Lin, X. Zhang, B. Zhao, T. Liu, Y. Yang, Z. Li, X. Zhou, X. Gao, Introduction of the X-ray diffraction beamline of SSRF, Nucl. Sci. Tech. 26 (2015), 020101.
[26] M. Gao, Y. Gu, L. Li, Z. Gong, X. Gao, W. Wen, Facile usage of a MYTHEN 1K with a Huber 5021 diffractometer and angular calibration in operando experiments, J. Appl. Crystallogr. 49 (2016) 1182–1189.
[27] B.H. Toby, EXPGUI, a graphical user interface for GSAS, J. Appl. Crystallogr. 34 (2001) 210–213.
[28] A.C. Larson, R.B. Von Dreele, General structure analysis system (GSAS), Los Alamos Natl. Lab. Rep. LAUR, 2004 86-748.
[29] E. Kroumova, M.I. Aroyo, J.M. Perez Mato, A. Kirov, C. Capillas, S. Ivantchev, H. Wondratschek, Bilbao Crystallographic Server II Representations of crystallographic point groups and space groups, Phase, Transit. 76 (2003) 155–170.
[30] P. Prokupková, P. Mošner, L. Koudelka, M. Vlček, Preparation and study of $Ca_{1-x}Mg_x(PO_3)_2$ glassy and crystalline phases, J. Mater. Sci. 33 (1998) 743–748.
[31] C. Calvo, The crystal structure of α-$Mg_2P_2O_7$, Acta Crystallogr. 23 (1967) 289–295.
[32] C. Calvo, Refinement of the crystal structure of β-$Mg_2P_2O_7$, Can. J. Chem. 43 (1965) 1139–1146.
[33] A.G. Nord, P. Kierkegaard, The crystal structure of $Mg_3(PO_4)_2$, Acta Chem. Scand. 22 (1968) 1466–1474.
[34] F. Brunet, D. Vielzeuf, The farringtonite/$Mg_3(PO_4)_2$-II transformation: a new curve for pressure calibration in piston-cylinder apparatus, Eur. J. Mineral. 8 (1996) 349–354.
[35] F. Brunet, C. Chopin, A. Elfakir, M. Quarton, Crystal and powder XRD data of $Mg_3(PO_4)_2$-III: High-temperature and high-pressure form, Powder Diffr. 10 (1995) 293–295.
[36] K.K. Mishra, S.N. Achary, S. Chandra, T.R. Ravindran, A.K. Sinha, M.N. Singh, A. K. Tyagi, Structural and thermal properties of $BaTe_2O_6$: Combined variable-temperature synchrotron X-ray diffraction, Raman spectroscopy, and ab initio calculations, Inorg. Chem. 55 (2016) 8994–9005.
[37] Y. Fei, Thermal Expansion, in: J.T. Ahrens (Ed.), Mineral Physics and Crystallography, American Geophysical Union, Washington D.C., 1995, 29-44.
[38] T. Okada, T. Narita, T. Nagai, T. Yamanaka, Comparative Raman spectroscopic study on ilmenite-type $MgSiO_3$ (akimotoite), $MgGe_O3$, and $MgTi_O3$ (geikielite) at high temperatures and high pressures, Am. Mineral. 93 (2008) 39–47.
[39] P. Gillet, F. Guyot, J.M. Malezieux, High-pressure, high-temperature Raman spectroscopy of Ca_2GeO_4 (olivine form): some insights on anharmonicity, Phys. Earth Planet. Inter. 58 (1989) 141–154.